Communication in Physical Sciences, 2025, 12(3) 1005-1026

Straight Line Solutions and their Stability of Libration Points with Oblateness Primaries and Circumbinary Disc in the Elliptic R3BP

Bashir Umar, Kamfa A Salisu & Mustapha Muhammad Sani
Received: 20 January 2025/Accepted: 02 March 2025/Published: 14 March 2025
https://dx.doi.org/10.4314/cps.v12i3.24

Abstract: *This study investigates the dynamical behavior and linear stability of the collinear Lagrangian point L3L_3L3 in the elliptic restricted three-body problem under the influence of perturbative parameters including the semi-major axis aaa, orbital eccentricity eee, and the oblateness A1A_1A1 of the more massive primary. For fixed values of A= 0 .01, A_2 = 0.022, M_b=0.01 and T=0.01, the location and stability of L_3 were examined numerically over varying conditions. Results show that as the semi-major axis decreases from 0.90 to 0.60, the coordinate L_3 shifts from –1.06706 to –0.964238, with the corresponding increase in the instability measure $\Omega^o_{\xi\xi}$ $\Omega^o_{\eta\eta}$ from –1.76868 to –2.25071. A similar trend is observed with increasing eccentricity from 0.10 to 0.40, where the coordinate of L_3 shifts from –1.08021 to –1.02960, while the instability measure increases from –1.58050 to –2.08276. Additionally, increasing the oblateness A_1 from 0.0001 to 0.2 causes the position of L_3 to shift from –1.04760 to –1.09594, while the instability product increases significantly from –1.79718 to –2.19480. These results confirm that L_3 is inherently unstable and increasingly sensitive to variations in orbital and physical parameters. The findings offer essential insights for mission planning and the stability analysis of celestial systems influenced by such perturbations.*

Keywords: *Circumbinary Disc – ER3BP – Oblateness – Collinear points*

Bashir Umar
Department of IJMB, School of Advanced and General Studies, Nuhu Bamalli Polytechnic, Zaria, Nigeria
Email: fbashumar@gmail.com

Kamfa A. Salisu
Department of Mathematics, Faculty of Physical Sciences, Ahmadu Bello University, Zaria, Nigeria
Email: salisukamfaabdulkadir@yahoo.com

Mustapha Muhammad Sani
Department of IJMB, School of Advanced and General Studies, Nuhu Bamalli Polytechnic, Zaria, Nigeria
Email: mmsani20@nubapoly.edu.ng

1 0 Introduction

The elliptic restricted three-body problem (ER3BP) describes the motion of an infinitesimal mass under the gravitational influence of two massive primary bodies orbiting their common barycenter in elliptic Keplerian orbits. This problem serves as a more realistic model than its circular counterpart because most celestial bodies in binary systems follow elliptic rather than circular orbits. In this dynamical system, five classical equilibrium points—three collinear (L_1,L_2, and L_3,) two triangular (L_4 and ,L_5)—exist. The collinear points lie along the line connecting the two primaries, while the triangular points form equilateral triangles with the primaries. These points play a significant role in space dynamics, mission planning, and celestial mechanics. However, the collinear points are generally linearly unstable, while the triangular points may be stable or unstable depending on the mass ratio of the primaries.

Over the years, several researchers have extended the classical ER3BP to incorporate more realistic factors, such as radiation pressure, oblateness of the primaries, and additional gravitational potentials. Sahoo and Ishwar (2000) studied the ER3BP with a

smaller oblate and radiating primary and confirmed the instability of the collinear points. Singh and Umar (2012, 2014) analyzed the system with both primaries being luminous and oblate, and showed that while the locations of the collinear points are affected by oblateness, eccentricity, and radiation pressure, the points remain linearly unstable. Similarly, Singh and Taura (2013, 2015) incorporated the gravitational potential from a circumbinary disc and higher-order oblateness (up to the zonal harmonic J4J_4J4) and demonstrated that new collinear points could emerge under such conditions, though most remain unstable. More recently, Hussain et al. (2018) examined systems like CEN X-4 and PSR J1903+0327 and reported the influence of triaxiality and oblateness on the collinear points in elliptic binary systems.

Circumbinary discs—ring-like distributions of material around binary stars—have been observed in numerous stellar systems and analogously exist in the Kuiper Belt of our own solar system (Luu & Jewitt, 2002). The gravitational potential generated by such discs introduces additional perturbations to the dynamical system and can significantly alter the number and location of equilibrium points (Jiang & Yeh, 2003; Yeh & Jiang, 2006; Kushvah, 2008). Therefore, considering the presence of a circumbinary disc is crucial in gaining deeper insight into the stability landscape of the ER3BP.

Despite the advancements in the literature, most existing studies have primarily focused on either circular orbits or neglected the combined effects of oblateness and circumbinary discs in elliptic configurations. Moreover, while additional collinear points have been identified in earlier models, their stability under the influence of both oblateness and disc potential in an elliptic frame remains inadequately explored.

This study aims to investigate the influence of the oblateness of the primaries and the gravitational potential of a surrounding circumbinary disc on the locations and linear stability of collinear libration points in the ER3BP. Specifically, we examine the emergence of new collinear equilibrium points and assess their dynamical behavior under perturbations. The significance of this study lies in its potential applications to celestial mechanics, particularly in understanding the dynamics of dust particles, asteroid belts, or spacecraft in binary star systems with extended mass distributions. It also contributes to theoretical advancements by bridging the gap between classical models and real-world astrophysical conditions.

1.1 Equations of motion

The equations of motion of the elliptic restricted three - body problem (ER3BP) when both primaries are oblate spheroids surrounded by a circumbinary disc in a dimensionless - pulsating coordinate system (ξ, η, ς) following Singh and Umar (2012) and Singh and Taura (2014) are:

$$\begin{aligned} &\xi'' - 2\eta' = \Omega_{\xi}, \\ &\eta'' + 2\xi' = \Omega_{\eta}, \\ &\varsigma'' = \Omega_{\varsigma}. \end{aligned} \tag{1}$$

With the force function

$$\Omega = \frac{1}{\left(1-e^2\right)^{\frac{1}{2}}}\left[\frac{\xi^2+\eta^2}{2} + \frac{1}{n^2}\left\{\frac{(1-\mu)}{r_1} + \frac{\mu}{r_2} + \frac{(1-\mu)A_1}{2r_1^3} + \frac{\mu A_2}{2r_2^3} + \frac{M_b}{\left(r^2+T^2\right)^{\frac{1}{2}}}\right\}\right] \tag{2}$$

The mean motion, n, is given by

$$n^2 = \frac{1}{a}\left(1+\frac{3e^2}{2}+\frac{3A_1}{2}+\frac{3A_2}{2}+\frac{2M_b r_c}{\left(r_c^2+T^2\right)^{\frac{3}{2}}}\right)$$

(3)

$$r_i^2 = (\xi-\xi_i)^2+\eta^2+\zeta^2 \qquad i=1,2; \quad \xi_1=-\mu \quad \xi_2=1-\mu$$

$$\mu = \frac{m_2}{m_1+m_2} \tag{4}$$

where $\frac{M_b}{\left(r_c^2+T^2\right)^{\frac{1}{2}}}$ is the potential due to the disc (Miyamoto & Nagai 1975; Singh and Taura 2013), where M_b is the total mass of the disc, r is the radial distance of the infinitesimal body and is given by $r^2=\xi^2+\eta^2$, $T=b+d$, b and d are parameter which determine the density profile of the circular cluster of material points. The parameter b controls the flatness of the profile and is known as the flatness parameter. The parameter d controls the size of the core of the density profile and is called the core parameter when $b=d=0$, the potential equals to the one by a point mass, r_c is the radial distance of the infinitesimal body in the classical restricted and n, a, e, A are the mean motion, semi – major axis, eccentricities of the orbits, oblateness respectively in 3BP. And the prime represents differentiation with respect to the eccentric anomaly E which describes the position of a particle moving along an elliptic keplerian orbit.

2.0 Locations of the Collinear Libration Points

The positions of the collinear points are the solution of the first derivative of equation (2) with respect to $\xi, \eta \; and \; \zeta$ respectively. That is $\Omega_\xi = \Omega_\eta = \Omega_\zeta = 0$ since the collinear points lie only on the ξ axis, it implies that $\eta = \zeta = 0$ on the system i.e

$$\Omega_\xi = \frac{1}{(1-e^2)^{\frac{1}{2}}}\left[\xi-\frac{1}{n^2}\left\{\frac{(1-\mu)(\xi+\mu)}{r_1^3}+\frac{\mu(\xi+\mu-1)}{r_2^3}+\frac{3(1-\mu)A_1(\xi+\mu)}{2r_1^5}+\frac{3\mu A_2(\xi+\mu-1)}{2r_2^5}+\frac{M_b\xi}{(r^2+T^2)^{\frac{3}{2}}}\right\}\right]=0$$

$$\Omega_\eta = \frac{1}{(1-e^2)^{\frac{1}{2}}}\eta\left[1-\frac{1}{n^2}\left\{\frac{(1-\mu)}{r_1^3}+\frac{\mu}{r_2^3}+\frac{3(1-\mu)A_1}{2r_1^5}+\frac{3\mu A_2}{2r_2^5}+\frac{M_b}{(r^2+T^2)^{\frac{3}{2}}}\right\}\right]=0$$

$$\Omega_\zeta = \frac{1}{(1-e^2)^{\frac{1}{2}}}\left[\frac{-\zeta}{n^2}\left\{\frac{(1-\mu)}{r_1^3}+\frac{\mu}{r_2^3}+\frac{3(1-\mu)A_1}{2r_1^5}+\frac{3\mu A_2}{2r_2^5}+\frac{M_b}{(r^2+T^2)^{\frac{3}{2}}}\right\}\right]=0 \tag{5}$$

From equation (4), when $\eta = \zeta = 0$

$$|r_1|^2 = |\xi+\mu|^2 \qquad |r_2|^2 = |\xi+\mu-1|^2 \tag{6}$$

$$\xi n^2 - \frac{(1-\mu)(\xi+\mu)}{|\xi+\mu|^3}-\frac{\mu(\xi+\mu-1)}{|\xi+\mu-1|^3}-\frac{3(1-\mu)A_1(\xi+\mu)}{2|\xi+\mu|^5}-\frac{3\mu A_2(\xi+\mu-1)}{2|\xi+\mu-1|^5}-\frac{M_b\xi}{(\xi^2+T^2)^{\frac{3}{2}}}=0 \tag{7}$$

To locate the straight line solutions on the line joining the primaries, the orbital plane is divided into three interval regions $\left(\xi_2 < L_1,\ \xi_1 < L_i\,(i=2,a,b) < \xi_2,\ \ L_3 < \xi_1\right)$ with respect t the primaries. The collinear points $L_i\,(i=1,2,\ a,b,3)$ lie in the these regions.

We consider the collinear points L_i*(i = 1,2,3,a, b)* in their respective intervals.

Case 1: Location of L_1

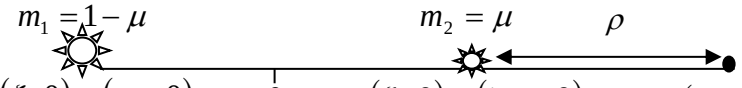

Figure 1: **ec**

Considerin $L_1 < \xi_2$, v the p f L_1

From figure 1, we can see $L_1 - \xi_2 = \rho, \quad L_1 - \xi_1 = 1+\rho \quad \Rightarrow L_1 = 1+\rho+\xi_1$

Now, from (6), we have $r_1 = 1+\rho$ and $r_2 = \rho$ then substituting in equation (7) gives;

$$2n^2(1+\rho-\mu)(1+\rho)^4\rho^4[(1+\rho-\mu)^2+T^2]^{\frac{3}{2}} - 2(1-\mu)(1+\rho)^2\rho^4[(1+\rho-\mu)^2 + T^2]^{\frac{3}{2}} - 2\mu(1+\rho)^4\rho^2[(1+\rho-\mu)^2+T^2]^{\frac{3}{2}} - 3(1-\mu)A_1\rho^4[(1+\rho-\mu)^2+T^2]^{\frac{3}{2}} - 3\mu A_2(1+\rho)^4[(1+\rho-\mu)^2+T^2]^{\frac{3}{2}} - 2M_b(1+\rho-\mu)(1+\rho)^4\rho^4 = 0 \quad (8)$$

Case 2: Location of L_i (i=2,a,b)

In the interval $(\xi_1 < L_i \ (i=2,a,b) < \xi_2)$, which correspond to L_i (i=2,a,b)

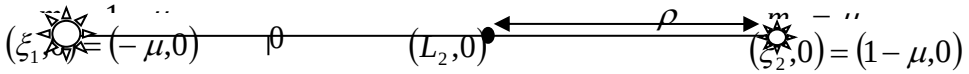

Figure 2: Location of the collinear equilibrium point L_2

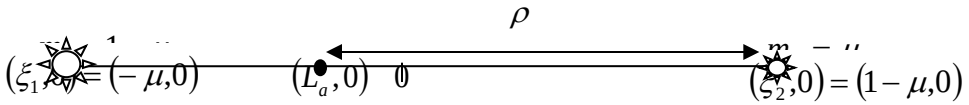

Figure 3: Location of the collinear equilibrium point L_a

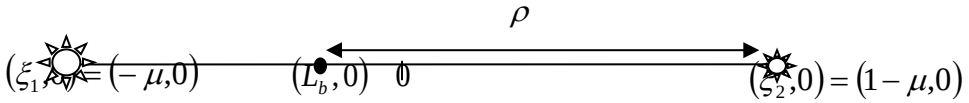

Figure 4: Location of the collinear equilibrium point L_b

From figures 2 - 4, we obtain, $\xi_2 - L_i(i=2,a,b) = \rho$

$L_i(i=2,a,b) - \xi_1 = 1-\rho \ \Rightarrow \ L_i(i=2,a,b) = 1-\rho-\mu$

Then, from (6) we obtain, $r_1 = 1-\rho$, $r_2 = \rho$

substituting in the above in equation (7) yields

$$2n^2(1-\rho-\mu)(1-\rho)^4\rho^4[(1-\rho-\mu)^2+T^2]^{\frac{3}{2}} - 2(1-\mu)(1-\rho)^2\rho^4[(1-\rho-\mu)^2 + T^2]^{\frac{3}{2}} + 2\mu(1-\rho)^4\rho^2[(1-\rho-\mu)^2+T^2]^{\frac{3}{2}} - 3(1-\mu)A_1\rho^4[(1-\rho-\mu)^2+T^2]^{\frac{3}{2}} + 3\mu A_2(1-\rho)^4[(1-\rho-\mu)^2+T^2]^{\frac{3}{2}} - 2M_b(1-\rho-\mu)(1-\rho)^4\rho^4 = 0 \quad (9)$$

Case 2: Location of L_3 $(\xi_1 > L_3)$

In the last interval $\xi_1 > L_3$,

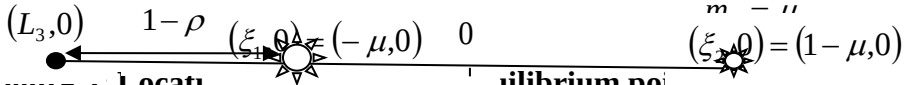

Figure 5: Location of the collinear equilibrium po

From figure: 5 we have; $\xi_1 - L_3 = 1-\rho,\ and\ \ \xi_2 - L_3 = 2-\rho$

and from (6), we have $r_1 = 1-\rho;\ r_2 = 2-\rho$

Putting in the above equations in (7) we have;

$$2n^2(\rho-1-\mu)(1-\rho)^4(2-\rho)^4[(\rho-1-\mu)^2+T^2]^{\frac{3}{2}} + 2(1-\mu)(1-\rho)^2(2-\rho)^4[(\rho-1-\mu)^2+T^2]^{\frac{3}{2}} + 2\mu(1-\rho)^4(2-\rho)^2[(\rho-1-\mu)^2+T^2]^{\frac{3}{2}} + 3(1-\mu)A_1(2-\rho)^4[(\rho-1-\mu)^2+T^2]^{\frac{3}{2}} + 3\mu A_2(1-\rho)^4[(\rho-1-\mu)^2+T^2]^{\frac{3}{2}} - 2M_b(\rho-1-\mu)(1-\rho)^4(2-\rho)^4 = 0 \quad (10)$$

3.0 Stability of the collinear equilibrium points

To investigates the stability of the collinear libration points L_i *(i=1,2,3,a,b)*; we consider the characteristic equation of the system in Singh and Umar (2012) given by

$$\lambda^4 - \left(\Omega^0_{\xi\xi} + \Omega^0_{\eta\eta} - 4\right)\lambda^2 + \Omega^0_{\xi\xi}\Omega^0_{\eta\eta} - \left(\Omega^0_{\xi\eta}\right)^2 = 0 \quad (11)$$

Now, we obtain the points corresponding to the collinear by taking the second partial derivatives of equation (2), with $\eta = 0$. Thus we have

$$\Omega_{\xi\xi} = \frac{1}{\left(1-e^2\right)^{\frac{1}{2}}}\left[1+\frac{2}{n^2}\left\{\frac{(1-\mu)}{|\xi+\mu|^3} + \frac{\mu}{|\xi+\mu-1|^3} + \frac{3(1-\mu)A_1}{|\xi+\mu|^5} + \frac{3\mu A_2}{|\xi+\mu-1|^5} - \frac{M_b}{2\left(\xi^2+T^2\right)^{\frac{3}{2}}} + \frac{3M_b\xi^2}{2\left(\xi^2+T^2\right)^{\frac{5}{2}}}\right\}\right]$$

$$\Omega_{\eta\eta} = \frac{1}{\left(1-e^2\right)^{\frac{1}{2}}}\left[1-\frac{1}{n^2}\left\{\frac{(1-\mu)}{|\xi+\mu|^3} + \frac{\mu}{|\xi+\mu-1|^3} + \frac{3(1-\mu)A_1}{2|\xi+\mu|^5} + \frac{3\mu A_2}{2|\xi+\mu-1|^5} + \frac{M_b}{\left(\xi^2+T^2\right)^{\frac{3}{2}}}\right\}\right]$$

$$\Omega_{\xi\eta} = \Omega_{\eta\xi} = 0$$

$$\Omega_{\zeta\zeta} = 0 \quad (12)$$

Since $\frac{3M_b\xi^2}{2\left(\xi^2+T^2\right)^{\frac{5}{2}}} > \frac{M_b}{2\left(\xi^2+T^2\right)^{\frac{3}{2}}}$ and the remaining terms are all positive, this implies that

$\Omega^0_{\xi\xi} > 0$

3.1 Stability of $L_1\left(\xi > \xi_2\right)$

In this case, we have; $r_1 = \xi+\mu \quad \Rightarrow \xi = r_1 - \mu$ and $r_2 = \xi+\mu-1$ (13)

With the use of equations (13) in equation (7) we obtain;

$$\frac{(1-\mu)}{r_1^2} = \left(\xi n^2 - \frac{\mu}{r_2^2} - \frac{3(1-\mu)A_1}{2r_1^4} - \frac{3\mu A_2}{2r_2^4} - \frac{M_b\xi}{\left(\xi^2+T^2\right)^{\frac{3}{2}}}\right) \quad (14)$$

Substituting equation (14) in the second equation of (12) gives;

$$\Omega_{\eta\eta}=\frac{1}{\left(1-e^2\right)^{\frac{1}{2}}}\left[1-\frac{1}{n^2}\left\{\frac{1}{r_1}\left(\xi n^2-\frac{\mu}{r_2^2}-\frac{3(1-\mu)A_1}{2r_1^4}-\frac{3\mu A_2}{2r_2^4}-\frac{M_b\xi}{\left(\xi^2+T^2\right)^{\frac{3}{2}}}\right)+\frac{\mu}{r_2^3}+\frac{3(1-\mu)A_1}{2r_1^5}+\frac{3\mu A_2}{2r_2^5}\right.\right.$$

$$\left.\left.+\frac{M_b}{\left(\xi^2+T^2\right)^{\frac{3}{2}}}\right\}\right]$$

Simplifying we have;

$$\Omega_{\eta\eta}=\frac{1}{\left(1-e^2\right)^{\frac{1}{2}}}\left[\frac{\mu}{r_1}+\frac{1}{n^2}\left\{\frac{\mu}{r_2^2}\left(\frac{1}{r_1}-\frac{1}{r_2}\right)+\frac{3\mu A_2}{2r_2^4}\left(\frac{1}{r_1}-\frac{1}{r_2}\right)+\frac{M_b(r_1-\mu)}{\left[(r_1-\mu)^2+T^2\right]^{\frac{3}{2}}}\left(\frac{1}{r_1}-\frac{1}{(r_1-\mu)}\right)\right\}\right]$$

Thus, $\Omega_{\eta\eta}^0<0$. Since $\mu<\frac{1}{2}$ $A_i(i=1,2)\ll 1$,$r_1>1$ and $r_2<1$

3.2 Stability of $L_i(i=2,a,b)$ in the interval $(\xi_1<\xi<\xi_2)$

In this interval, we have; $r_1=(\xi+\mu)\Rightarrow\xi=(r_1-\mu)$ and $r_2=-(\xi+\mu-1)$. (15)

Substituting equation (15) in the equation (7) yields

$$\frac{(1-\mu)}{r_1^2}=\left(\xi n^2+\frac{\mu}{r_2^2}-\frac{3(1-\mu)A_1}{2r_1^4}+\frac{3\mu A_2}{2r_2^4}-\frac{M_b\xi}{\left(\xi^2+T^2\right)^{\frac{3}{2}}}\right) \tag{16}$$

Substituting equation (16) in the second equation of (12) gives;

$$\Omega_{\eta\eta}=\frac{1}{\left(1-e^2\right)^{\frac{1}{2}}}\left[1-\frac{1}{n^2}\left\{\frac{1}{r_1}\left(\xi n^2+\frac{\mu}{r_2^2}-\frac{3(1-\mu)A_1}{2r_1^4}+\frac{3\mu A_2}{2r_2^4}-\frac{M_b\xi}{\left(\xi^2+T^2\right)^{\frac{3}{2}}}\right)+\frac{\mu}{r_2^3}+\frac{3(1-\mu)A_1}{2r_1^5}+\right.\right.$$

$$\left.\left.+\frac{M_b}{\left(\xi^2+T^2\right)^{\frac{3}{2}}}\right\}\right] \tag{17}$$

Which implies that;

$$\Omega_{\eta\eta}=\frac{1}{\left(1-e^2\right)^{\frac{1}{2}}}\left[\frac{\mu}{r_1}-\frac{1}{n^2}\left\{\frac{\mu}{r_2^2}\left(\frac{1}{r_1}+\frac{1}{r_2}\right)+\frac{3\mu A_2}{2r_2^4}\left(\frac{1}{r_1}+\frac{1}{r_2}\right)-\frac{M_b(r_1-\mu)}{\left[(r_1-\mu)^2+T^2\right]^{\frac{3}{2}}}\left(\frac{1}{r_1}-\frac{1}{(r_1-\mu)}\right)\right\}\right]$$

Thus, $\Omega_{\eta\eta}^0<0$, Since $\mu<\frac{1}{2}$, $A_i(i=1,2)<<1$, $r_1>1$ and $r_2>1$

3.3 Stability of $L_3(\xi_1>\xi)$

In the last interval, we have; $r_1=-(\xi+\mu)\Rightarrow\xi=-(r_1+\mu)$ and $r_2=-(\xi+\mu-1)$. (18)

Substituting equation (18) in the equation (7) yields

$$\frac{(1-\mu)}{r_1^2} = -\left(\xi n^2 + \frac{\mu}{r_2^2} + \frac{3(1-\mu)A_1}{2r_1^4} + \frac{3\mu A_2}{2r_2^4} - \frac{M_b \xi}{\left(\xi^2 + T^2\right)^{\frac{3}{2}}} \right) \tag{19}$$

Substituting equation (19) in the second equation of (12) gives;

$$\Omega_{\eta\eta} = \frac{1}{\left(1-e^2\right)^{\frac{1}{2}}} \left[1 - \frac{1}{n^2} \left\{ -\frac{1}{r_1} \left(\xi n^2 + \frac{\mu}{r_2^2} + \frac{3(1-\mu)A_1}{2r_1^4} + \frac{3\mu A_2}{2r_2^4} - \frac{M_b \xi}{\left(\xi^2 + T^2\right)^{\frac{3}{2}}} \right) + \frac{\mu}{r_2^3} + \frac{3(1-\mu)A_1}{2r_1^5} + \right.\right.$$

$$\left.\left. + \frac{M_b}{\left(\xi^2 + T^2\right)^{\frac{3}{2}}} \right\} \right] \tag{20}$$

Simplifying we get;

$$\Omega_{\eta\eta} = \frac{1}{\left(1-e^2\right)^{\frac{1}{2}}} \left[-\frac{\mu}{r_1} + \frac{1}{n^2} \left\{ \frac{\mu}{r_2^2} \left(\frac{1}{r_1} - \frac{1}{r_2} \right) + \frac{3\mu A_2}{2r_2^4} \left(\frac{1}{r_1} - \frac{1}{r_2} \right) + \frac{M_b (r_1 + \mu)}{\left[(r_1 + \mu)^2 + T^2 \right]^{\frac{3}{2}}} \left(\frac{1}{r_1} - \frac{1}{(r_1 + \mu)} \right) \right\} \right]$$

$\Omega_{\eta\eta}^0 < 0$, Since $\mu < \frac{1}{2}$, $A_i (i = 1,2) << 1$, $r_1 > 1$ and $r_2 < 1$

Clearly, $\Omega_{\xi\xi}^0 > 0$, $\Omega_{\eta\eta}^0 < 0$, and $\Omega_{\xi\eta}^0 = 0$.

Since, $\Omega_{\xi\xi}^0 \Omega_{\eta\eta}^0 - \Omega_{\xi\eta}^0 < 0$, the discriminant of equation (11) is positive.

4.0 Results and Discussion

In this numerical investigation, the influence of various dynamical parameters on the collinear equilibrium points Li (where i=1,2,3,,a, b) is presented in detail through a series of tabulated data. These parameters include the oblateness of the primary bodies, the semi-major axis, the eccentricity of the orbit, and the mass of a surrounding belt or disc. The equilibrium positions, denoted by ρLi\rho_{L_i}ρLi, and the corresponding second-order derivatives of the potential function Ω(ξ,η), specifically $\Omega_{\xi\xi}^o$ and $\Omega_{\eta\eta}^o$ are studied to understand their impact on the location and linear stability of these points.

Table 1 presents the effect of varying the semi-major axis on the position and stability of the collinear point L_1. For a fixed eccentricity e=0.3, oblateness coefficients $A_1 = 0.0025$ and A_2=0.0002, belt mass M_b=0.5 and other parameters, the semi-major axis was varied from 0.90 to 0.60.

Table1: Effect of semi- major axis on *L_1* for *A_1=0.01, A_2=0.02, M_b=0.01, T=0.01* and *e = 0.3*

a	ρL_1	L_1	$\Omega_{\xi\xi}^0$	$\Omega_{\eta\eta}^0$	$\Omega_{\xi\xi}^0 \Omega_{\eta\eta}^0$	$\lambda_{1,2}$	$\lambda_{3,4}$	Remark
0.90	0.54173	1.19173	5.48768	-0.99446	-5.45730	± 1.61111	± 1.44998i	Unstable
0.85	0.52889	1.17889	5.57564	-1.02705	-5.72648	± 1.63798	± 1.46095i	Unstable
0.80	0.515642	1.16564	5.67210	-1.06246	-6.02639	± 1.66690	± 1.47272i	Unstable
0.75	0.501948	1.15195	5.77844	-1.10111	-6.36271	± 1.69816	± 1.48540i	Unstable
0.70	0.487762	1.13776	5.89642	-1.14354	-6.74278	± 1.73213	± 1.49913i	Unstable

0.65	0.473032	1.12303	6.02821	-1.19038	-7.17585	± 1.76925	± 1.51407i	Unstable
0.60	0.457694	1.10769	6.17664	-1.24245	-7.67418	± 1.81009	± 1.53044i	Unstable

From Table 1, it is evident that as the semi-major axis decreases, the value of ρL_1 reduces progressively, indicating that the collinear point L_1 shifts inward toward the smaller primary. This shift is accompanied by an increase in the magnitude of the curvature terms $\Omega^o_{\xi\xi}$ and $\Omega^o_{\eta\eta}$, resulting in a stronger restoring force in the ξ\ direction and greater instability in the η-direction. The roots remain purely imaginary throughout, indicating that the motion around L_1 is unstable under small perturbations. Table 2 indicates that increasing the oblateness of the bigger primary results in a continuous inward shift of the equilibrium point L_1. Simultaneously, the curvature of the potential increases, leading to a more unstable configuration, as seen in the higher imaginary components of the roots. This implies that the flattened shape of the bigger primary enhances the gravitational asymmetry in the system. As shown in Table 3, increasing the oblateness of the smaller primary causes the point L_1 to move outward from the smaller primary. However, the magnitude of the potential's second derivatives decreases, slightly reducing the degree of instability, though the roots remain imaginary, indicating persistent instability.

From Table 4, it is clear that as the belt mass increases, ρL_1 reduces significantly, and the potential curvature steepens in both directions. The increasing imaginary values of the roots confirm that the belt mass induces greater gravitational asymmetry and instability near L_1The data in Table 5 highlight that increasing orbital eccentricity also causes an inward shift of L_1, with a steepening of the potential gradient.

Table 2: Effect of oblateness of the bigger primary on L_1 for A_2=0.02, M_b=0.01, T=0.01, a=0.85 and e = 0.3

A_1	ρL_1	L_1	$\Omega^0_{\xi\xi}$	$\Omega^0_{\eta\eta}$	$\Omega^0_{\xi\xi}\Omega^0_{\eta\eta}$	$\lambda_{1,2}$	$\lambda_{3,4}$	Remark
0.0001	0.531408	1.18141	5.55934	-1.02187	-5.68091	± 1.6332	± 1.4594i	Unstable
0.001	0.531177	1.18118	5.56083	-1.02234	-5.68508	± 1.6336	± 1.4595i	Unstable
0.01	0.528890	1.17889	5.57564	-1.02705	-5.72648	± 1.6379	± 1.4609i	Unstable
0.1	0.507919	1.15792	5.71761	-1.07166	-6.12733	± 1.6791	± 1.4742i	Unstable
0.2	0.487987	1.13799	5.86345	-1.11654	-6.54680	± 1.7202	± 1.4874i	Unstable

Table 3: Effect of oblateness of the smaller primary on L_1 for A_1=0.02, M_b=0.01, T=0.01, a=0.90 and e = 0.25

A_2	ρL_1	L_1	$\Omega^0_{\xi\xi}$	$\Omega^0_{\eta\eta}$	$\Omega^0_{\xi\xi}\Omega^0_{\eta\eta}$
0.0002	0.534442	1.18444	5.05521	-0.97461	-4.92688
0.002	0.535711	1.18571	5.08779	-0.97367	-4.95385
0.02	0.547016	1.19702	5.37112	-0.96571	-5.18694
0.1	0.579802	1.22980	6.14278	-0.94772	-5.82166
0.2	0.603079	1.25308	6.66849	-0.93992	-6.26787

This leads to higher instability, indicated by increasingly large imaginary components of the characteristic roots. The investigation also covers the behavior of equilibrium point L_2, summarized in Tables 6 to 9, which similarly reflect the impact of varying M_b, A_2, A_1, and e

respectively. The shift in L_2 toward the barycenter and the rising curvature of the potential signify that increased belt mass intensifies the instability of L_2, as reflected in the larger imaginary components of the roots. Subsequent tables follow the same pattern of interpretation, confirming that increased values of oblateness and eccentricity generally destabilize the equilibrium points by altering the geometry and depth of the gravitational potential. From Table 7, as A_2 increases, the position of L_2 moves outward (increase in ρL_2 and closer to the smaller primary (decrease in L_2. This shift results in significantly increased values of the second derivatives of the effective potential Ω, reflecting enhanced dynamical instability around L_2. The product $\Omega^o_{\xi\xi}\ \Omega^o_{\eta\eta}$ becomes more negative, confirming increased sensitivity to perturbations. This table examines how varying the oblateness coefficient A1A_1A1 of the bigger primary affects L_2, with parameters A_2=0.02, M_b=0.01, T=0.01, a=0.85a = 0.85, and e=0.3. The data (Table 8) reveals that increasing A_1 causes a reduction in ρL_2 and a corresponding increase in L_2, signifying that the Lagrangian point shifts away from the bigger primary. A stronger oblateness effect in the bigger primary intensifies the gravitational influence, altering the equilibrium point's location and increasing instability, as seen from the more negative product of the second derivatives.

Table 4: Effect of belt on L_1 for A_1=0.01, A_2=0.02, T=0.01, a=0.90 and e = 0.3

M_b	ρL_1	L_1	$\Omega^0_{\xi\xi}$	$\Omega^0_{\eta\eta}$	$\Omega^0_{\xi\xi}\Omega^0_{\eta\eta}$
0.01	0.541730	1.19173	5.48768	-0.99446	-5.45730
0.1	0.510883	1.16088	5.61603	-1.03695	-5.82355
0.2	0.483903	1.13390	5.73759	-1.07570	-6.17194
0.3	0.462135	1.11213	5.84271	-1.10803	-6.47391
0.4	0.444058	1.09406	5.93525	-1.13557	-6.73990
0.5	0.428712	1.07871	6.01783	-1.15942	-6.97717

Table 5: Effect of eccentricity on L_1 for A_1=0.01, A_2=0.02, T=0.01, a=0.85 and M_b = 0.01

e	ρL_1	L_1	$\Omega^0_{\xi\xi}$	$\Omega^0_{\eta\eta}$	$\Omega^0_{\xi\xi}\Omega^0_{\eta\eta}$
0.10	0.552701	1.20270	5.19304	-0.92795	-4.81889
0.15	0.548732	1.19873	5.25059	-0.94302	-4.95142
0.20	0.543338	1.19334	5.33250	-0.96436	-5.14245
0.25	0.536668	1.18667	5.44015	-0.99224	-5.39790
0.30	0.528890	1.17889	5.57564	-1.02705	-5.72648
0.35	0.520187	1.17019	5.74179	-1.06937	-6.14011
0.40	0.510743	1.16074	5.94246	-1.11998	-6.65543

Table 6: Effect of Circumbinary disk on L_2 for A_1=0.01, A_2=0.02, T=0.01, a=0.90 and e = 0.3

M_b	ρL_2	L_2	$\Omega^0_{\xi\xi}$	$\Omega^0_{\eta\eta}$	$\Omega^0_{\xi\xi}\Omega^0_{\eta\eta}$
0.01	0.438722	0.211273	17.5034	-6.53984	-114.470
0.1	0.386552	0.263448	23.3139	-9.22091	-214.975
0.2	0.356792	0.293208	25.3493	-10.0515	-254.799

0.3	0.336810	0.313190	26.2402	-10.3500	-271.587
0.4	0.321788	0.328212	26.6786	-10.4486	-278.754
0.5	0.309798	0.340202	26.8995	-10.4568	-281.283

Table 7: Effect of oblateness of the smaller primary on L_2 for $A_1=0.02$, $M_b=0.01$, $T=0.01$, $a=0.90$ and $e = 0.25$

A_2	ρL_2	L_2	$\Omega^0_{\xi\xi}$	$\Omega^0_{\eta\eta}$	$\Omega^0_{\xi\xi}\Omega^0_{\eta\eta}$
0.0002	0.419424	0.230576	16.3645	-6.38943	-104.560
0.002	0.420944	0.229056	16.5572	-6.42573	-106.392
0.02	0.434200	0.215800	18.1888	-6.74659	-122.712
0.1	0.471657	0.178343	22.3962	-7.70741	-172.617
0.2	0.499190	0.15081	25.2428	-8.51551	-214.955

Table 8: Effect of oblateness of the bigger primary on L_2 for $A_2=0.02$, $M_b=0.01$, $T=0.01$, $a=0.85$ and $e = 0.3$

A_1	ρL_2	L_2	$\Omega^0_{\xi\xi}$	$\Omega^0_{\eta\eta}$	$\Omega^0_{\xi\xi}\Omega^0_{\eta\eta}$
0.0001	0.443806	0.206134	16.2169	-6.08139	-98.6212
0.001	0.443399	0.206601	16.2514	-6.08475	-98.8855
0.01	0.439469	0.210531	16.5836	-6.11856	-101.468
0.1	0.409553	0.240447	19.0009	-6.42088	-122.003
0.2	0.387328	0.262672	20.5627	-6.63975	-136.531

Table 9 shows the dependence of the location and stability of L_2 on the orbital eccentricity e, with fixed values: A_1=0.01, A_2=0.02, T=0.01, a=0.85, and M_b=0.01.Table 9 investigates the impact of varying eccentricities (e) on L2L_2L2 for a set of fixed parameters (A_1=0.01, A_2=0.02, T=0.01, a=0.85, M_b = 0.01). The table shows that as the eccentricity increases from 0.10 to 0.40, the values of L_2 slightly decrease from 0.211863 to 0.209378, indicating a small but noticeable reduction in L_2 with higher eccentricity. The corresponding $\Omega^o_{\xi\xi}$ and $\Omega^o_{\eta\eta}$ values also show a trend of decreasing magnitudes, with $\Omega^o_{\xi\xi}$ decreasing from 17.5566 to 15.9588 and $\Omega^o_{\eta\eta}$ dropping from -6.62489 to -5.77214. This implies that the dynamical behavior of the system, in terms of its rotational and precessional motion, is less influenced by higher eccentricities. Additionally, the product$\Omega^o_{\xi\xi}$ $\Omega^o_{\eta\eta}$ consistently decreases, showing that the interaction between the rotational axes weakens with increasing eccentricity.

Table 10 examines how changing the semi-major axis (a) affects L_2 for fixed parameters (A_1=0.01, A_2=0.02, M_b = 0.01, T=0.01, and e=0.30). The table illustrates that as the semi-major axis decreases from 0.90 to 0.60, L_2 progressively decreases from 0.211273 to 0.205124. The corresponding values of $\Omega^o_{\xi\xi}$ and $\Omega^o_{\eta\eta}$ also decrease with decreasing semi-major axis. For example, $\Omega^o_{\xi\xi}$ decreases from 17.5034 to 12.0018, while $\Omega^o_{\eta\eta}$ decreases from -6.53969 to -4.01984. This suggests that the orbital

dynamics become less intense with a decreasing semi-major axis, leading to a reduction in the rotational behavior of the system. Furthermore, the product $\Omega^o_{\xi\xi}\Omega^o_{\eta\eta}$ consistently reduces, showing weaker interactions as the semi-major axis decreases.

Table 9: Effect of eccentricity on L_2 for A_1=0.01, A_2=0.02, T=0.01, a=0.85 and M_b = 0.01

e	ρL_2	L_2	$\Omega^0_{\xi\xi}$	$\Omega^0_{\eta\eta}$	$\Omega^0_{\xi\xi}\Omega^0_{\eta\eta}$
0.10	0.438137	0.211863	17.5566	-6.62489	-116.311
0.15	0.438346	0.211654	17.3839	-6.53680	-113.635
0.20	0.438638	0.211362	17.1556	-6.41938	-110.128
0.25	0.439013	0.210987	16.8841	-6.27793	-105.997
0.30	0.439469	0.210531	16.5836	-6.11856	-101.468
0.35	0.440006	0.209994	16.2697	-5.94774	-96.7682
0.40	0.440622	0.209378	15.9588	-5.77214	-92.1163

Table 10: Effect of semi- major axis on L_2 for A_1=0.01, A_2=0.02, M_b=0.01, T=0.01 and e = 0.3

a	ρL_2	L_2	$\Omega^0_{\xi\xi}$	$\Omega^0_{\eta\eta}$	$\Omega^0_{\xi\xi}\Omega^0_{\eta\eta}$
0.90	0.438727	0.211273	17.5034	-6.53969	-114.467
0.85	0.439469	0.210531	16.5836	-6.11856	-101.468
0.80	0.440298	0.209702	15.6648	-5.69778	-89.2544
0.75	0.441229	0.208771	14.7469	-5.27744	-77.8262
0.70	0.442284	0.207716	13.8303	-4.85760	-67.1821
0.65	0.443488	0.206512	12.9152	-4.43836	-57.3221
0.60	0.444876	0.205124	12.0018	-4.01984	-48.2452

Table 11 explores the effect of varying the mass of the belt (Mb) on LaL_aLa for a fixed set of parameters (A_1=0.01, A_2 = 0.02, T=0.01, a=0.90, e=0.30). As the mass of the belt increases from 0.01 to 0.5, the value of LaL_aLa becomes increasingly negative, starting at -0.000511 for M_b = 0.01 and reaching -0.000010 for M_b = 0.5. This suggests that the system becomes more "stiff" with increasing belt mass, which might indicate greater rigidity or resistance to deformation. The corresponding angular velocities $\Omega^o_{\xi\xi}$ and $\Omega^o_{\eta\eta}$ become more negative and larger in magnitude as the mass increases. For instance, $\Omega^o_{\xi\xi}$ a drops from -7699.33 to -190638, while $\Omega^o_{\eta\eta}$ follows a similar trend. This shows that the system's dynamics become more intense as the belt mass increases, likely due to an increase in inertia and rotational resistance.

Table 12 investigates the influence of the oblateness of the smaller primary (A2) on LaL_aLa for a set of fixed parameters (A_1=0.02, M_b = 0.01, T= 0.01, a=0.90, and e=0.25). As A_2 increases from 0.0002 to 0.2, L_a becomes slightly more negative, and $\Omega^o_{\xi\xi}$ decrease in magnitude. For example, $\Omega^o_{\xi\xi}$ decreases from -7920.62 to -6299.20, $\Omega^o_{\xi\xi}$ $\Omega^o_{\eta\eta}$ drops from -8057.49 to -6398.28. This

indicates that the oblateness of the smaller primary reduces the system's precession and rotational motion as its magnitude increases. The uct $\Omega_{\xi\xi}^{o}\Omega_{\eta\eta}^{o}$ also decreases as A_2 increases, suggesting a weaker interaction between the rotational axes as the oblateness of the smaller primary grows.

Table 13 explores how the oblateness of the larger primary (A_1) affects L_a for fixed parameters (A_2=0.02, M_b=0.01, T=0.01, a=0.85, and e=0.30). As A_1 increases from 0.0001 to 0.2, the values of L_a shift from -0.000445 to -0.001870, indicating a more negative L_a. The angular velocities $\Omega_{\xi\xi}^{o}$ and $\Omega_{\eta\eta}^{o}$ also decrease in magnitude as A1 increases, with $\Omega_{\xi\xi}^{o}$ decreasing from -7388.80 to -4988.56 and $\Omega_{\eta\eta}^{o}$ decreasing from -7470.44 to -5708.03. The product $\Omega_{\xi\xi}^{o}\Omega_{\eta\eta}^{o}$ also decreases, confirming that the system's dynamics become less intense as the oblateness of the bigger primary increases.

Table 14 examines the effect of eccentricity (e) on L_a for a set of fixed parameters (A_1=0.01, A_2=0.02, T=0.01, a=0.85, M_b = 0.01). The values of L_a remain constant at -0.000511 as eccentricity increases from 0.10 to 0.40, suggesting that the eccentricity does not influence La. However, $\Omega_{\xi\xi}^{o}$ and $\Omega_{\eta\eta}^{o}$ change as eccentricity increases. For instance, $\Omega_{\xi\xi}^{o}$ decreases from -7742.08 to -6962.14, and $\Omega_{\eta\eta}^{o}$decreases from -7849.95 to -7059.16. This shows that while eccentricity does not affect L_a , it does influence the precession and rotational motion of the system.

Finally, Table 15 investigates the effect of varying the semi-major axis (a) on L_a for fixed parameters (A_1=0.01, A_2=0.02, M_b=0.01, T=0.01, and e=0.30). As the semi-major axis decreases from 0.90 to 0.60, L_a remains constant at -0.000511. However, $\Omega_{\xi\xi}^{o}$ and $\Omega_{\eta\eta}^{o}$ decrease in magnitude, with $\Omega_{\xi\xi}^{o}$ changing from -7699.33 to -5132.54 and $\Omega_{\eta\eta}^{o}$ changing from -7806.62 to -5204.06. This indicates that decreasing the semi-major axis results in weaker rotational and precessional motions. The product $\Omega_{\xi\xi}^{o}$ $\Omega_{\eta\eta}^{o}$ also decreases, reinforcing the idea that the system's dynamics are less intense with a decreasing semi-major axis.

Table 11: Effect of belt on L_a for A_1=0.01, A_2=0.02, T=0.01, a=0.90 and e = 0.3

M_b	ρL_a	L_a	$\Omega_{\xi\xi}^{0}$	$\Omega_{\eta\eta}^{0}$	$\Omega_{\xi\xi}^{0}\Omega_{\eta\eta}^{0}$
0.01	0.650511	-0.000511	-7699.33	-7806.62	2.22479×10^{29}
0.1	0.650051	-0.000051	-65534.3	-65578.7	4.29769×10^{9}
0.2	0.650025	-0.000025	-111119	-111153	1.23512×10^{10}
0.3	0.650017	-0.000017	-144639	-144669	2.09247×10^{10}
0.4	0.650013	-0.000013	-170326	-170352	2.90153×10^{10}
0.5	0.650010	-0.000010	-190638	-190661	3.63472×10^{10}

Table 12: Effect of oblateness of the smaller primary on L_a for A_1=0.02, M_b=0.01, T=0.01, a=0.90 and e = 0.25

A_2	ρL_a	L_a	$\Omega_{\xi\xi}^{0}$	$\Omega_{\eta\eta}^{0}$	$\Omega_{\xi\xi}^{0}\Omega_{\eta\eta}^{0}$
0.0002	0.650583	-0.000583	-7920.62	-8057.49	6.38203×10^{7}
0.002	0.650583	-0.000583	-7902.03	-8038.64	6.35216×10^{7}
0.02	0.650578	-0.000578	-7722.92	-7855.37	6.06664×10^{7}
0.1	0.650554	-0.000554	-7017.35	-7133.11	5.00555×10^{7}

0.2	0.650524	-0.000524	-6299.20	-6398.28	4.0304×10^7

Table 13: Effect of oblateness of the bigger primary on L_a for $A_2=0.02$, $M_b=0.01$, $T=0.01$, $a=0.85$ and $e = 0.3$

A_1	ρL_a	L_a	$\Omega^0_{\xi\xi}$	$\Omega^0_{\eta\eta}$	$\Omega^0_{\xi\xi}\Omega^0_{\eta\eta}$
0.0001	0.650445	-0.000445	-7388.80	-7470.44	5.51976×10^7
0.001	0.650451	-0.000451	-7378.14	-7461.50	5.5052×10^7
0.01	0.650511	-0.000511	-7271.54	-7372.86	5.3612×10^7
0.1	0.651125	-0.001125	-6203.03	-6543.55	4.05899×10^7
0.2	0.65187	-0.001870	-4988.56	-5708.03	2.84748×10^7

Table 14: Effect of eccentricity on L_a for $A_1=0.01$, $A_2=0.02$, $T=0.01$, $a=0.85$ and $M_b = 0.01$

e	ρL_a	L_a	$\Omega^0_{\xi\xi}$	$\Omega^0_{\eta\eta}$	$\Omega^0_{\xi\xi}\Omega^0_{\eta\eta}$
0.10	0.650511	-0.000511	-7742.08	-7849.95	6.0775×10^7
0.15	0.650511	-0.000511	-7659.15	-7765.88	5.948×10^7
0.20	0. 650511	-0.000511	-7549.23	-7654.42	5.77849×10^7
0.25	0. 650511	-0.000511	-7417.87	-7521.23	5.57915×10^7
0.30	0. 650511	-0.000511	-7271.54	-7372.86	5.3612×10^7
0.35	0. 650511	-0.000511	-7117.20	-7216.37	5.13604×10^7
0.40	0. 650511	-0.000511	-6962.14	-7059.16	4.91469×10^7

Table 15: Effect of semi- major axis on L_a for $A_1=0.01$, $A_2=0.02$, $M_b=0.01$, $T=0.01$ and $e = 0.3$

a	ρL_a	L_a	$\Omega^0_{\xi\xi}$	$\Omega^0_{\eta\eta}$	$\Omega^0_{\xi\xi}\Omega^0_{\eta\eta}$
0.90	0.650511	-0.000511	-7699.33	-7806.62	6.01057×10^7
0.85	0.650511	-0.000511	-7372.54	-7372.86	5.3612×10^7
0.80	0.650511	-0.000511	-6843.74	-6939.10	4.74894×10^7
0.75	0.650511	-0.000511	-6415.94	-6505.34	4.17378×10^7
0.70	0.650511	-0.000511	-5988.14	-6071.58	3.63575×10^7
0.65	0.650511	-0.000511	-5560.34	-5637.82	3.13482×10^7
0.60	0.650511	-0.000511	-5132.54	-5204.06	2.67101×10^7

The data from these tables provide important insights into the orbital and dynamical behavior of the system as different parameters are varied. From the above, it is evidence that,

(i) Eccentricity and semi-major axis have significant effects on L_2, with higher eccentricities and smaller semi-major axes leading to a decrease in L_2 and a corresponding reduction in the dynamical intensity.

(ii) Increasing the mass of the belt and the oblateness of the primary bodies significantly affects L_a, leading to a more negative L_a and a stronger interaction between the rotational axes.

(iii) The influence of eccentricity on L_a appears to be minimal, as L_a remains constant despite changes in eccentricity.

These results provide useful information for understanding the dynamics of the system

under various orbital and physical configurations.

Table 16 shows how the value of L_b changes with varying M_b (belt mass). As the value of M_b increases, both ρL_b and L_b exhibit a steady increase. The angular velocities $\Omega^o_{\xi\xi}$ and $\Omega^o_{\eta\eta}$ exhibit varying trends, with $\Omega^o_{\xi\xi}$ decreasing slightly as M_b increases, while $\Omega^o_{\eta\eta}$ decreases significantly. This suggests that the impact of increasing belt mass is primarily felt in the reduction of angular velocity terms. Table 17: Effect of Oblateness of the Smaller Primary on L_b for A_1=0.02, M_b=0.01, T=0.01T = 0.01, a=0.90 , and e=0.25. Table 17shows results for the investigation of the effect of the oblateness of the smaller primary (controlled by A_2) on L_b . As A_2 increases, both ρL_b show a very small increase. This indicates that the oblateness of the smaller primary has a minimal effect on the linear size L_b. The angular velocities $\Omega^o_{\xi\xi}$ and $\Omega^o_{\eta\eta}$ show a decrease with increasing A_2, with $\Omega^o_{\xi\xi}$ decreasing more significantly than $\Omega^o_{\eta\eta}$.

Table 18: Effect of Oblateness of the Bigger Primary on L_b for A_2 = 0.02, M_b = 0.01, T=0.01T = 0.01, a=0.85, and e=0.3/ Table 18 explores the effect of the oblateness of the bigger primary on L_b. As A_1 increases, ρL_b and L_b both show a decreasing trend, indicating that increasing the oblateness of the bigger primary reduces the values of these parameters. The angular velocities $\Omega^o_{\xi\xi}$ and $\Omega^o_{\eta\eta}$ show significant increases with increasing A_1, particularly with $\Omega^o_{\xi\xi}$, which increases substantially when A_1 reaches higher values.

Table 19: Effect of Eccentricity on L_b for A_1 = 0.01, A_2=0.02, T=0.01, a = 0.85, and M_b = 0.01. Table 19 shows the effect of eccentricity (e) on L_b. As eccentricity increases, both ρL_b and L_b remain almost constant, with only very slight changes observed. The angular velocities $\Omega^o_{\xi\xi}$ and $\Omega^o_{\eta\eta}$ decrease steadily as eccentricity increases, suggesting that increasing eccentricity results in a gradual decrease in the overall angular velocities. Table 20: Effect of Semi-Major Axis on L_b for A_1 = 0.01, A_2 = 0.02, M_b = 0.011T=0.01, and e=0.3. Table 20 examines the influence of the semi-major axis (aaa) on LbL_bLb. As the semi-major axis decreases from 0.90 to 0.60, both ρL_b and L_b show a minimal decrease. The angular velocities $\Omega^o_{\xi\xi}$ and $\Omega^o_{\eta\eta}$ decrease substantially with a decrease in the semi-major axis, especially $\Omega^o_{\xi\xi}$, which decreases significantly as the semi-major axis becomes smaller.

Table 21: Effect of Oblateness of the Smaller Primary on L_3 for A_1 = 0.02, M_b = 0.01, T=0.01T = 0.01, a = 0.90, and e=0.25. Table 21 investigates the effect of the oblateness of the smaller primary on L_3. As A_2 increases, both ρL_3 exhibit a small but steady increase. This suggests that the oblateness of the smaller primary has a moderate effect on the size of L_3 . The angular velocities $\Omega^o_{\xi\xi}$ and $\Omega^o_{\eta\eta}$ also show a slight increase with increasing A_2, though the effect is not as pronounced. Table 22: Effect of Belt on L_3 for A_1 = 0.01, A_2 = 0.02, T=0.01, a = 0.90 , and e=0.3. Table 22 analyzes the impact of the belt mass (M_b) on L_3. As M_b increases, both ρL_3 and L_3 show a clear increase. This suggests that a higher belt mass leads to an increase in the size of L_3. The angular velocities $\Omega^o_{\eta\eta}$ show small fluctuations as M_b increases, with $\Omega^o_{\xi\xi}$ remaining largely unaffected and $\Omega^o_{\xi\xi}$ and $\Omega^o_{\eta\eta}$ displaying a slight increase as the belt mass increases. In summary, the data in Tables 16 to 22 show that the parameters L_b_ and L_3 are influenced by several factors, including the mass of the belt, the oblateness of the primaries, eccentricity, and the semi-major axis. In general, the increase in belt mass leads to an increase in both L_b and L_3, while other factors such as eccentricity and oblateness have varying effects, generally resulting in minor to moderate changes in these values.

Table 16: Effect of belt on L_b for A_1=0.01, A_2=0.02, T=0.01, a=0.90 and e = 0.3

M_b	ρL_b	L_b	$\Omega^0_{\xi\xi}$	$\Omega^0_{\eta\eta}$	$\Omega^0_{\xi\xi}\Omega^0_{\eta\eta}$
0.01	0.686124	-0.036124	311.281	-167.372	-52099.6
0.1	0.742462	-0.092462	234.970	-111.653	-26235.1
0.2	0.765962	-0.115962	228.642	-105.790	-24188.1
0.3	0.780691	-0.130691	225.687	-102.548	-23143.7
0.4	0.791414	-0.141414	223.456	-100.071	-22361.5
0.5	0.799813	-0.149813	221.565	-98.0087	-21715.3

Table 17: Effect of oblateness of the smaller primary on L_b for A_1=0.02, M_b=0.01, T=0.01, a=0.90 and e = 0.25

A_2	ρL_b	L_b	$\Omega^0_{\xi\xi}$	$\Omega^0_{\eta\eta}$	$\Omega^0_{\xi\xi}\Omega^0_{\eta\eta}$
0.0002	0.683741	-0.033741	381.957	-206.91	-79030.8
0.002	0.68375	-0.033750	380.874	-206.294	-78571.9
0.02	0.683839	-0.033839	370.344	-200.311	-74184.2
0.1	0.684242	-0.034242	328.875	-176.767	-58134.4
0.2	0.684757	-0.034757	286.883	-152.971	-43884.8

Table 18: Effect of oblateness of the bigger primary on L_b for A_2=0.02, M_b=0.01, T=0.01, a=0.85 and e = 0.3

A_1	ρL_b	L_b	$\Omega^0_{\xi\xi}$	$\Omega^0_{\eta\eta}$	$\Omega^0_{\xi\xi}\Omega^0_{\eta\eta}$
0.0001	0.688921	-0.038921	244.415	-131.268	-32083.9
0.001	0.688637	-0.038637	248.996	-133.696	-33289.9
0.01	0.686117	-0.036117	294.167	-158.089	-46504.8
0.1	0.673703	-0.023703	701.366	-420.000	-294574
0.2	0.667697	-0.017697	1045.40	-750.655	-784735

Table 19: Effect of eccentricity on L_b for A_1=0.01, A_2=0.02, T=0.01, a=0.85 and M_b = 0.01

e	ρL_b	L_b	$\Omega^0_{\xi\xi}$	$\Omega^0_{\eta\eta}$	$\Omega^0_{\xi\xi}\Omega^0_{\eta\eta}$
0.10	0.686129	-0.036129	312.866	-168.293	-52653.1
0.15	0.686127	-0.036127	309.569	-166.496	-51542.0
0.20	0.686125	-0.036125	305.187	-164.105	-50082.5
0.25	0.686121	-0.036121	299.978	-161.264	-48375.6
0.30	0.686117	-0.036117	294.167	-158.089	-46504.8
0.35	0.686111	-0.036111	288.069	-154.757	-44580.6
0.40	0.686105	-0.036105	281.942	-151.401	-42686.2

Table 20: Effect of semi- major axis on L_b for A_1=0.01, A_2=0.02, M_b=0.01, T=0.01 and e = 0.3

a	ρL_b	L_2	$\Omega^0_{\xi\xi}$	$\Omega^0_{\eta\eta}$	$\Omega^0_{\xi\xi}\Omega^0_{\eta\eta}$
0.90	0.686124	-0.036124	311.281	-167.372	-52099.6

0.85	0.686117	-0.036117	294.167	-158.089	-46504.8
0.80	0.686108	-0.036108	277.072	-148.820	-41233.7
0.75	0.686099	-0.036099	259.959	-139.537	-36274.2
0.70	0.686089	-0.036089	242.841	-130.253	-31630.7
0.65	0.686077	-0.036077	225.73	-120.972	-27307.1
0.60	0.686063	-0.036063	208.619	-111.692	-23301.1

Table 21: Effect of oblateness of the smaller primary on L_3 for $A_1=0.02$, $M_b=0.01$, $T=0.01$, $a=0.90$ and $e = 0.25$

A_2	ρL_3	L_3	$\Omega^0_{\xi\xi}$	$\Omega^0_{\eta\eta}$	$\Omega^0_{\xi\xi}\Omega^0_{\eta\eta}$
0.0002	0.263321	-1.08668	4.07243	-0.414368	-1.68749
0.002	0.263946	-1.08605	4.07356	-0.414749	-1.68951
0.02	0.270090	-1.07991	4.08482	-0.418520	-1.70958
0.1	0.295199	-1.05480	4.13293	-0.434472	-1.79564
0.2	0.322383	-1.02762	4.18912	-0.452782	-1.89675

Table 22: Effect of belt on L_3 for $A_1=0.01$, $A_2=0.02$, $T=0.01$, $a=0.90$ and $e = 0.3$

M_b	ρL_3	L_3	$\Omega^0_{\xi\xi}$	$\Omega^0_{\eta\eta}$	$\Omega^0_{\xi\xi}\Omega^0_{\eta\eta}$
0.01	0.282937	-1.06706	4.09109	-0.432326	-1.76868
0.1	0.316156	-1.03384	4.10160	-0.435122	-1.78470
0.2	0.345076	-1.00492	4.10661	-0.435455	-1.78824
0.3	0.368284	-0.98172	4.10698	-0.433912	-1.78207
0.4	0.387447	-0.96255	4.10420	-0.431147	-1.76951
0.5	0.403621	-0.94638	4.09900	-0.427572	-1.75273

As shown in Table 23, a decrease in the semi-major axis aaa from 0.90 to 0.60 leads to an increase in the distance ρL_3, indicating that the libration point L_3 shifts away from the system's barycenter. Concurrently, the x-coordinate of L_3 becomes less negative, suggesting a shift toward the origin. The radial curvature of the potential, represented by $\Omega^o_{\xi\xi}$ increases with decreasing a, while the transverse curvature $\Omega^o_{\eta\eta}$ becomes more negative. This divergence results in a more negative product $\Omega^o_{\xi\xi}\Omega^o_{\eta\eta}$, reflecting increased instability at L_3. These results imply that a shorter orbital path, corresponding to a smaller semi-major axis, exacerbates the disparity in potential curvature and leads to greater dynamical instability at the libration point.

In Table 24, the effect of varying orbital eccentricity eee from 0.10 to 0.40 is presented. As e increases, the value of ρL_3 also increases, showing that L_3 moves farther away from the barycenter. The coordinate L_3 becomes less negative, again indicating a drift toward the central mass. The parameter $\Omega^o_{\xi\xi}$ increases with increasing eccentricity, while $\Omega^o_{\eta\eta}$ becomes increasingly negative. Consequently, the product $\Omega^o_{\xi\xi}\Omega^o_{\eta\eta}$ becomes more negative, further confirming that greater orbital eccentricity enhances the instability of L_3. This suggests that higher orbital eccentricity introduces more asymmetry in the force

distribution around L_3, leading to reduced stability.

Table 25 explores the effect of the oblateness of the bigger primary body, represented by A_1, on the location and stability of L_3. As A_1 increases from 0.0001 to 0.2, the value of ρL_3 decreases, indicating that the libration point shifts closer to the barycenter. Simultaneously, the x-coordinate of L_3 becomes more negative, signifying a shift toward the larger primary. The radial curvature $\Omega_{\xi\xi}^{o}$ shows a substantial increase, while the transverse curvature and $\Omega_{\eta\eta}^{o}$ becomes slightly less negative. The product and $\Omega_{\eta\eta}^{o}$ becomes increasingly negative with higher oblateness, suggesting that the perturbing influence of the larger primary's shape intensifies the instability of the libration point. This indicates that greater oblateness amplifies the perturbative forces acting on the system, drawing L_3 closer to the larger mass and enhancing its dynamical instability.

Taken together, the results from Tables 23 to 25 confirm that the position and stability of the collinear libration point L_3 are highly sensitive to variations in semi-major axis, eccentricity, and the oblateness of the larger primary. In all scenarios, L_3 remains an unstable equilibrium point, as evidenced by the consistently negative values of $\Omega_{\eta\eta}^{o}$ and the increasingly negative product $\Omega_{\xi\xi}^{o}\Omega_{\eta\eta}^{o}$. These findings are important for understanding the dynamic environment around L_3 and for assessing its suitability for potential applications such as spacecraft positioning.

Table 23: Effect of semi- major axis on L_3 for $A_1=0.01$, $A_2=0.02$, $M_b=0.01$, $T=0.01$ and $e = 0.3$

a	ρL_3	L_3	$\Omega_{\xi\xi}^{0}$	$\Omega_{\eta\eta}^{0}$	$\Omega_{\xi\xi}^{0}\Omega_{\eta\eta}^{0}$
0.90	0.282937	-1.067060	4.09109	-0.432326	-1.76868
0.85	0.298399	-1.051600	4.11907	-0.444185	-1.82963
0.80	0.314440	-1.035560	4.14960	-0.457063	-1.89663
0.75	0.331121	-1.018880	4.18310	-0.471116	-1.97073
0.70	0.348510	-1.001490	4.22008	-0.486540	-2.05324
0.65	0.366690	-1.983310	4.26118	-0.503577	-2.14583
0.60	0.385762	-0.964238	4.30726	-0.522540	-2.25071

Table 24: Effect of eccentricity on L_3 for $A_1=0.01$, $A_2=0.02$, $T=0.01$, $a=0.85$ and $M_b = 0.01$

e	ρL_3	L_3	$\Omega_{\xi\xi}^{0}$	$\Omega_{\eta\eta}^{0}$	$\Omega_{\xi\xi}^{0}\Omega_{\eta\eta}^{0}$
0.10	0.269788	-1.08021	3.90048	-0.405206	-1.58050
0.15	0.274538	-1.07546	3.93317	-0.411124	-1.61702
0.20	0.281005	-1.06900	3.97980	-0.419509	-1.66957
0.25	0.289023	-1.06098	4.04133	-0.430475	-1.73969
0.30	0.298399	-1.05160	4.11907	-0.444185	-1.82963
0.35	0.308927	-1.04107	4.21488	-0.460873	-1.94253
0.40	0.320396	-1.02960	4.33127	-0.480865	-2.08276

Table 25: Effect of oblateness of the bigger primary on L_3 for $A_2=0.02$, $M_b=0.01$, $T=0.01$, $a=0.85$ and $e = 0.3$

A_1	ρL_3	L_3	$\Omega^0_{\xi\xi}$	$\Omega^0_{\eta\eta}$	$\Omega^0_{\xi\xi}\Omega^0_{\eta\eta}$
0.0001	0.302401	-1.04760	4.03717	-0.445160	-1.79718
0.001	0.302024	-1.04798	4.04489	-0.445066	-1.80024
0.01	0.298399	-1.05160	4.11907	-0.444185	-1.82963
0.1	0.271999	-1.07800	4.65725	-0.438893	-2.04403
0.2	0.254059	-1.09594	5.02791	-0.436500	-2.19480

As e increases, the location ρL_2 gradually increases while L_2 decreases, signifying a small yet consistent outward drift. The decreasing product of $\Omega^o_{\xi\xi}$ a $\Omega^o_{\eta\eta}$ indicates a reduction in instability, highlighting the stabilizing effect of higher eccentricity in this model configuration. Furthermore, as illustrated in Tables 10 to 14, varying the oblateness coefficients and the semi-major axis causes distinct changes in the second-order derivatives and the effective potential, which further contribute to the stability of the system. These effects underscore the intricate interplay between various parameters in determining the overall stability of the libration points in the restricted three-body system, and thus have important implications for celestial mechanics and orbital dynamics in systems with similar configurations. The findings presented in Tables 8 to 14 highlight that perturbations from various sources (such as increased belt mass, eccentricity, and oblateness) have a profound impact on the position and stability of the libration points, with clear trends of destabilization for extreme values of these parameters. The sensitivity of the system to these perturbations must be considered for practical applications in celestial navigation, satellite placement, and understanding the dynamics of multi-body systems.

The four subplots in the provided figure visually present how the position of collinear Lagrangian points L_1, L_2, and L_3 responds to variations in three key system parameters: eccentricity eee, oblateness A_1, and semi-major axis aaa. The horizontal axis in all plots denotes the x-coordinate ξ\xiξ of the collinear points, while the vertical axes represent the changing parameters under study. Each Lagrange point is marked using a distinct color and symbol for clarity: blue circles for L_1, red stars for L_2, yellow circles for L_3, and green circles for L_2 in some plots (possibly redundant labeling of L_2, unless it refers to the retrograde motion or another configuration).

Fig. 1a shows how the x-coordinate ξ\xiξ of each Lagrange point shifts as the eccentricity eee increases from 0.10 to 0.45. The points shift rightward on the x-axis, indicating an outward movement from the barycenter for all three collinear points. The trend is most pronounced for L (yellow), which moves significantly with increasing eccentricity. This observation is consistent with Table 24, which shows that ρL_3 increases and the x-coordinate of L_3 becomes less negative with increasing e, indicating that the point shifts farther from the barycenter. The effect of increasing oblateness A_1 from 0.0001 to 0.20 on the x-position of collinear points is illustrated in Fig. 1b

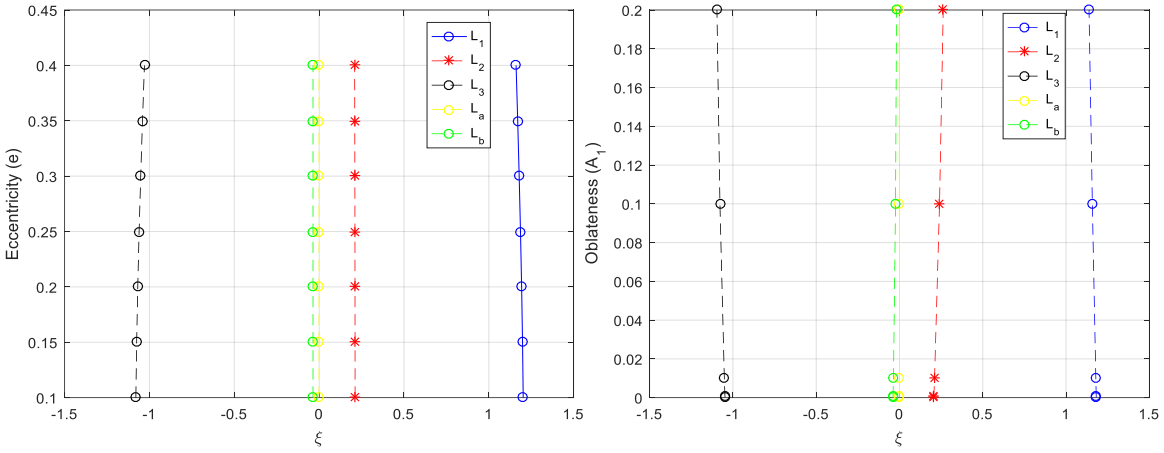

(a) (b)

Fig. 1 Effects of eccentricity (a) and oblateness (b) on the collinear libration points$L_i(i = 1, 2, 3, a, b)$.

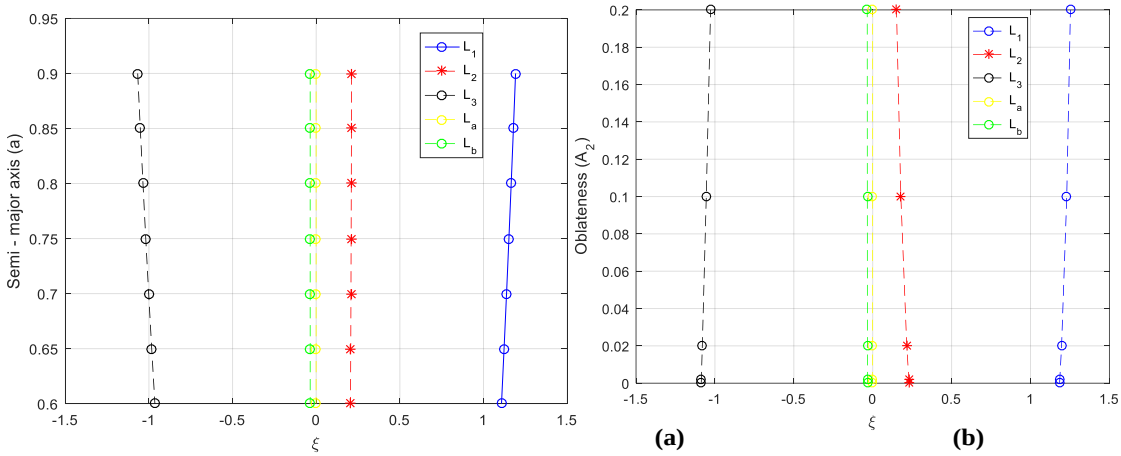

(a) (b)

Fig. 2: Effects of semi-major axis (a) and oblateness (b) on the collinear libration points$L_i(i = 1, 2, 3, a, b)$

As $A_1$1 increases, L_3 (yellow) clearly shifts leftward (toward the larger primary), as shown by a more negative x-coordinate. This is consistent with the trend in Table 25, where increasing oblateness draws L_3 closer to the barycenter, with a corresponding decrease in ρL_3 and more negative x-coordinates. Interestingly, L_1 and L_2 also appear to shift slightly, but their movements are more stable compared to L_3.Here, the vertical axis represents the semi-major axis a, ranging from 0.60 to 0.90. As a decreases, L_3 (yellow) moves farther from the origin, with its x-coordinate becoming less negative. This implies that for tighter orbits (smaller a), the collinear point shifts outward. This trend matches the data in Table 23, where decreasing aaa corresponds to increased ρL_3 and x-values that approach zero, again indicating outward drift of L_3. This behavior reflects the increased dominance of the centrifugal force in more compact orbits.

This subplot reiterates the impact of A_1 on the collinear points. The trends match those in the top right figure and Table 25. The x-coordinate of L_3 becomes more negative with increasing A_1, confirming the tendency of the point to

move closer to the more oblate primary. The clear and consistent leftward shift of L_3 under increasing oblateness emphasizes its sensitivity to the shape of the primary mass, a key finding also supported numerically in the table.

Across all four subplots, L_3 consistently exhibits the most significant positional shifts in response to changes in orbital and system parameters, confirming its inherently unstable nature. This is backed by the tabular results, where the product $\Omega^o_{\xi\xi}\Omega^o_{\eta\eta}$ becomes increasingly negative with changes in aaa, eee, and A_1, reinforcing the notion of growing instability. Visually, the consistent outward or inward migration of L3L_3L3 across parameters further illustrates the numerical trends.

In contrast, L_1 and L_2 appear more stable, with minor positional changes despite parameter variations. This reflects their relatively more balanced force environments. In conclusion, the visual and tabular data are in strong agreement: L_3 is most sensitive to changes in semi-major axis, eccentricity, and oblateness, and consistently displays behavior that aligns with increasing dynamical instability. These findings have practical implications for spacecraft mission planning and modeling of perturbed celestial systems.

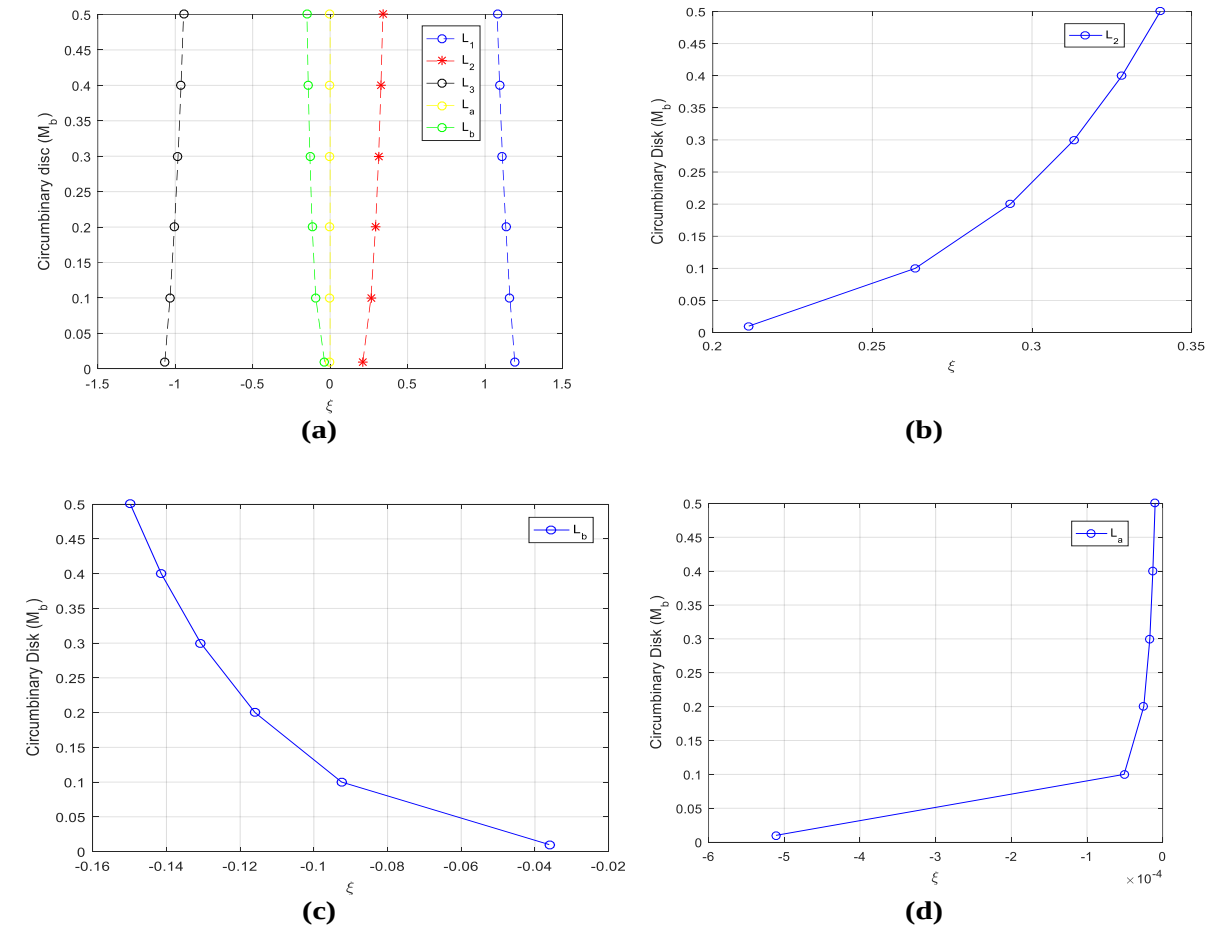

Fig. 2: **Effects of circumbinary disk on the collinear libration points$L_i(i = 1, 2, 3, a, b)$**

Fig. 2 provides similar information to those shown in in the Tables.

5.0 Conclusion

The study revealed that the positions and stability of the collinear Lagrangian point L_3 are highly sensitive to variations in the semi-

major axis aaa, eccentricity e, and oblateness A_1 of the primaries. As the semi-major axis decreases, the x-coordinate of L_3 becomes less negative, indicating a shift away from the barycenter, which corresponds to an increase in distance and instability. Similarly, as the eccentricity increases, L_3 moves farther away, further indicating sensitivity to orbital elongation. In contrast, an increase in oblateness of the primary leads to a reduction in the x-coordinate of L_3, drawing it closer to the more oblate body and also enhancing its instability. The product $\Omega^o_{\xi\xi}\Omega^o_{\eta\eta}$, which serves as an indicator of local stability, becomes more negative with increasing perturbations in these parameters, confirming that L_3 is inherently unstable under such dynamical conditions. On the other hand, L_1 and L_2 showed minor variations in position and remained relatively stable in comparison to L_3.

Based on the results, it can be concluded that the dynamical behavior of collinear equilibrium points in the circular restricted three-body problem is significantly affected by orbital and physical perturbations, with L_3 being the most sensitive and unstable among them. These variations in behavior under changing conditions highlight the importance of accurate modeling in trajectory planning for space missions, especially those involving station-keeping near L_3 or in systems with pronounced oblateness and eccentricity.

It is recommended that further investigations should focus on the combined effects of additional perturbative forces such as radiation pressure and triaxiality, especially for systems with small mass ratios where such forces can be more prominent. Future studies should also explore non-linear stability analysis using Lyapunov exponents and extend the analysis to three-dimensional models to gain deeper insights into the motion around the collinear points. For mission design, it is advisable to avoid placing spacecraft at or near L_3 in systems where significant oblateness or eccentricity is present, and instead consider alternative configurations or stabilization techniques.

6.0 References

Aminu, A. H., Aishetu, U., & Singh, J. (2018). Investigation of the stability of a test particle in the vicinity of collinear points with the additional influence of an oblate primary and a triaxial-stellar companion in the frame of ER3BP. *International Frontier Science Letters,* 13, pp. 12–27.

Ammar, M. K. (2004). The effect of solar radiation pressure on the Lagrangian points in the elliptic restricted three-body problem. *Astrophysics and Space Science,* 313, 4, pp. 393–408.

Greaves, J. S., Holland, W. S., Moriarty-Schieven, G., et al. (1998). A dust ring around Eridani: Analog to the young solar system. *Astrophysical Journal, 506*, pp L133–L137.

Iorio, L. (2007). An assessment of the measurement of the Lense-Thirring effect in the Earth gravity field, with CHAMP and GRACE data. *Monthly Notices of the Royal Astronomical Society,* 375, 4, pp. 1311–1314.

Iorio, L. (2012). Planetary precessions and the Newtonian and non-Newtonian effects of general relativity. *Earth, Moon, and Planets*, 108, 3-4, pp. 189–217.

Jiang, I. G., & Yeh, L. C. (2003). Bifurcation for dynamical systems of planet–belt intersection. *International Journal of Bifurcation and Chaos,* 13, pp. 534–539.

Jiang, I. G., & Yeh, L. C. (2004a). The modified restricted three body problems. *Revista Mexicana de Astronomía y Astrofísica,* 21, pp. 152–155.

Jiang, I. G., & Yeh, L. C. (2004b). On the chaotic orbits of disk–star–planet systems. *Astronomical Journal,* 128, pp. 923–932.

Kumar, S., & Ishwar, B. (2011). Location of collinear equilibrium points in the generalized elliptic restricted three-body

problem. *International Journal of Engineering, Science and Technology, 3*,pp. 157–162.

Kushvah, B. S. (2008). Linear stability of equilibrium points in the generalized photogravitational Chermnykh's problem. *Astrophysics and Space Science, 318*, pp. 41–50.

Luu, J. X., & Jewitt, D. C. (2002). Kuiper belt objects: Relics from the accretion disk of the Sun. *Annual Review of Astronomy and Astrophysics, 40*, pp. 63–101. https://doi.org/10.1146/

Miyamoto, M., & Nagai, R. (1975). Three dimensional models for the distribution of mass in galaxies. *Publications of the Astronomical Society of Japan, 27*, pp. 533–543.

Singh, J., & Ishwar, B. (1999). Stability of triangular equilibrium points in the generalized photogravitational restricted three-body problem. *Bulletin of the Astronomical Society of India, 27*, 415–424.

Singh, J., & Taura, J. J. (2013). Motion in the generalized restricted three-body problem. *Astrophysics and Space Science, 343*, 95.

Singh, J., & Taura, J. J. (2015). Collinear libration points in the photogravitational CR3BP with zonal harmonics and potential from a belt. *International Journal of Astronomy and Astrophysics, 5*, 155–165. http://dx.doi.org/10.4236/ijaa.2015

Singh, J., & Umar, A. (2012). Collinear equilibrium points in the elliptic R3BP with radiation and oblateness. *Astrophysics and Space Science, 52*, 1489–1496. http://dx.doi.org/10.1016/j.asr.2013.07.027

Szebehely, V. (1967a). *Theory of orbits: The restricted problem of three bodies*. Academic Press.

Szebehely, V. (1967b). Stability of the points of equilibrium in the restricted problem. *Astronomical Journal, 72*, 7–9.

Trilling, D. E., Stansbery, J. A., Stapelfeld, K. R., et al. (2007). Debris disks in main-sequence binary systems. *Astrophysical Journal, 658*, 1289–1311.

Declaration

Consent for publication

Not applicable

Availability of data

The publisher has the right to make data public.

Competing interests

The authors declared no conflict of interest

Ethical Consideration

Not applicable

Funding

There is no source of external funding.

Authors' contributions

All the authors contributed to the work. BU designed the work while all other authors were involved in supervision and correction of the manuscript